Inverse Problems **10** (1994) 341–351. Printed in the UK

High-resolution electromagnetic imaging of the conductive Earth interior

Dominique Gibert†§, Benoît Tournerie†‖ and Jean Virieux‡¶

† Géosciences Rennes, Université Rennes 1, Campus de Beaulieu, 35042 Rennes cedex, France

‡ Institut de Géodynamique, CNRS, Avenue A Einstein, 06560 Valbonne, France

Received 15 July 1993

Abstract. Ohmic dissipation in conductive media considerably limits the penetrative power of high-frequency electromagnetic imaging methods and implies that deep regions can be probed only with low-frequency fields. Unfortunately, these low-frequency fields are governed by a diffusive equation which prevents direct high-resolution imaging as in seismic and georadar imaging. However, a clue for high-resolution imaging in the diffusive approximation is given by a Fredholm integral equation of the first kind which links diffusive fields to their propagative duals. If these duals could be recovered by inverting this integral equation, the seismic imaging toolbox might be used, at least from a theoretical point of view, to produce fine electromagnetic images. Spectral decomposition of the integral operator shows that the inverse problem is numerically ill-posed for both noisy and/or incomplete data. High-resolution can be achieved only by adding sparsity constraints upon the sought solution to the information content of the data. This type of *a priori* information also strongly regularizes the inversion but implies that the inverse problem must be treated as non-linear. A numerical algorithm, designed to work in a continuous parameter space, couples both the simulated annealing and the simplex to recover the propagative field. Numerical applications for pseudo-data with additive noise reveal that reflective interfaces can be imaged even within the poorly-favourable magnetotelluric setup.

1. Introduction

Imaging the Earth's interior is a major task in geophysics which involves different techniques depending on both the nature and the depth of the targets to detect. For instance, elastic body waves radiated from seismic regions are used to image the main discontinuities found in the whole Earth [7], long-period surface waves are an efficient tool to probe the upper mantle down to 700 km in depth [26], while artificially-created elastic waves constitute the preferred means to image the first kilometers of the subsurface in the context of petroleum exploration [4]. Another and growing field of interest in high-resolution imaging techniques is subsurface geophysics which involves areas such as prospecting for water resources, waste disposal and civil engineering. Up to now, the main operational imaging techniques used in shallow geophysics are seismic [20] and georadar [5] soundings which respectively use information carried by elastic waves and electromagnetic waves. While seismic imaging can be adapted to any penetration depth, the georadar suffers a dramatic limitation to its penetrating power due to ohmic dissipation. The basic reason for such a limitation comes

§ E-mail address: gibert@univ-rennes1.fr

‖ E-mail address: tourneri@univ-rennes1.fr

¶ E-mail address: viri@mimosa.unice.fr

0266-5611/94/020341+11$19.50

from the fact that rocks are electrical, conductive media inside which the electromagnetic field is governed by the telegrapher equation,

$$\nabla \times \nabla \boldsymbol{E}(\boldsymbol{r}, t) + \mu\varepsilon(\boldsymbol{r})\frac{\partial^2}{\partial t^2}\boldsymbol{E}(\boldsymbol{r}, t) + \mu\sigma(\boldsymbol{r})\frac{\partial}{\partial t}\boldsymbol{E}(\boldsymbol{r}, t) = \boldsymbol{S}(\boldsymbol{r}, t) \tag{1}$$

where μ, ε and σ stand for the magnetic permeability, and the electric permittivity and conductivity respectively. $\boldsymbol{S}(\boldsymbol{r}, t)$ represents a source term. General solutions to this equation are damped waves but in the Earth, where the conductivity is large, the wave-like character of the electromagnetic field disappears very quickly to the benefit of the diffusive behavior [29] and, for most geophysical models, the electromagnetic field is given by the diffusion equation,

$$\nabla \times \nabla \boldsymbol{E}(\boldsymbol{r}, t) + \mu\sigma(\boldsymbol{r})\frac{\partial}{\partial t}\boldsymbol{E}(\boldsymbol{r}, t) = \boldsymbol{S}(\boldsymbol{r}, t)\,. \tag{2}$$

High-resolution electromagnetic imaging in this diffusive context has long been considered as an impossible challenge, mainly for the theoretical reason that diffusion constitutes a formal barrier to any 'diffraction-like' tomography. Links exist, however, between diffusion and propagation [9, 17, 27] and their study could cast new insights upon the possibilities for high-resolution electromagnetic imaging in a diffusive context. The need for a detailed study of the transformation from a diffusive to a propagative field is further motivated by the fact that the state of the art of wave-field imaging, which is now well developed [3], might be used to the benefit of diffusive-field imaging if a bridge could be put between the two domains [38]. For instance, and to illustrate this strategy, it is well established that wave-field imaging does not allow for high-resolution reconstructions of the velocity distribution but does for the reflectivity (i.e. impedance gradients) [13]. This result is also valid for the diffusive case and indicates that imaging in terms of the conductivity distribution (the electromagnetic equivalent of seismic velocity) will not allow for a high resolution which could be reached only in terms of conductivity gradients (i.e. the equivalent of seismic reflectivity). This strongly guides the way to parametrize the inverse problem. The goals of this paper are both to precisely document the formal inversion from a diffusive to a propagative field and, then, to rely on this formal inverse to set up a practical numerical inversion which could operate on actual data. Section 2 documents the links between propagation and diffusion and solves the inverse problem of transforming a diffusive field into a propagative dual. Section 3 examines and discusses the various constraints we use to stabilize the inversion of incomplete and noisy data. A numerical solution using simulated annealing is presented in section 4, and realistic synthetic examples are presented in section 5. Although primarily designed for geophysical purposes this study also applies to other fields interested in imaging conductive media such as in non-destructive control and medical imaging [41, 42].

2. From a diffusive to a propagative field

To set a link between diffusion and propagation we follow the approach given in [19] which formally introduces a field satisfying the wave equation

$$\nabla \times \nabla \boldsymbol{U}(\boldsymbol{r}, q) + \mu\sigma(\boldsymbol{r})\frac{\partial^2}{\partial q^2}\boldsymbol{U}(\boldsymbol{r}, q) = \boldsymbol{F}(\boldsymbol{r}, q) \tag{3}$$

where q is an independent variable playing the role of pseudo-time with a physical dimension of square-root of time, and $\boldsymbol{F}(\boldsymbol{r}, q)$ is a source term. The wave speed $c(\boldsymbol{r}) = 1/\sqrt{\mu\sigma(\boldsymbol{r})}$. An integral equation between $\boldsymbol{E}(t)$ and $\boldsymbol{U}(q)$,

$$\boldsymbol{E}(t) = \int_0^\infty \frac{q}{2\sqrt{\pi t^3}} \exp\left(-\frac{q^2}{4t}\right) \boldsymbol{U}(q)\, \mathrm{d}q \tag{4}$$

introduces a kernel corresponding to the three-dimensional Green function of the diffusion equation. The spatial dependence of the fields has been left implicit since the transformation only involves the time t and the variable q. The source terms $\boldsymbol{S}(\boldsymbol{r}, t)$ and $\boldsymbol{F}(\boldsymbol{r}, q)$ are related by the same expression. The direct problem of transforming a propagative field into a diffusive one is numerically stable as one may expect from the damped nature of the integral kernel in (4), and the inverse transformation from a diffusive field $\boldsymbol{E}(\boldsymbol{r}, t)$ into its propagative dual $\boldsymbol{U}(\boldsymbol{r}, q)$ it must be stressed is highly unstable. This is more understandable in the Fourier domain ($t \longrightarrow \nu$) where (4) transforms into

$$\boldsymbol{E}(\nu) = \int_0^\infty \exp(-q\sqrt{\mathrm{i}\nu})\boldsymbol{U}(q)\, \mathrm{d}q\,. \tag{5}$$

This Fredholm equation posseses the nice property that its kernel only depends upon the product of the dual variables. Such a property is verified for many integral equations encountered in mathematical physics such as, for instance, in laser anemometry [23], light scattering by polydispersive media [30], and inverse diffraction [2]. Solutions of such dilationally-invariant Fredholm integral equations can be given under the form of an eigenfunction expansion [22]. Following this approach and looking for eigenfunctions Φ_ω verifying

$$\Phi_\omega(\nu) = \lambda_\omega^{-1} \int_0^\infty \exp(-q\sqrt{\mathrm{i}\nu})\Phi_\omega(q)\, \mathrm{d}q \tag{6}$$

we find the collection ($\omega \in \mathbb{R}^+$)

$$\Phi_\omega^+(s) = \frac{1}{\sqrt{\pi s}} \cos\left(\frac{\theta_\omega}{2} - \omega \ln s\right) \qquad \Phi_\omega^-(s) = \frac{1}{\sqrt{\pi s}} \sin\left(\frac{\theta_\omega}{2} - \omega \ln s\right) \tag{7}$$

where

$$\theta_\omega = \arg\left[\Gamma\left(\frac{1}{2} + \mathrm{i}\omega\right) \exp\left(\frac{\pi(\omega - \mathrm{i}/2)}{4}\right)\right] \tag{8}$$

and

$$\lambda_\omega^\pm = \pm\sqrt{\frac{\pi \exp(\frac{1}{2}\pi\omega)}{\cosh(\pi\omega)}}\,. \tag{9}$$

The set $\{\Phi_\omega^\pm, \omega \in \mathbb{R}^+\}$ constitutes an orthogonal basis when the functional space is equipped with the scalar product $(f, g) \equiv \int_0^\infty f(\xi)g(\xi)\, \mathrm{d}\xi$, and projecting† both the diffusive and the propagative fields upon this basis gives

$$\boldsymbol{U}(q) = \int_0^\infty \mathrm{d}\omega \frac{\Phi_\omega^\pm(q)}{\lambda_\omega^\pm} \int_0^\infty \boldsymbol{E}(\nu)\Phi_\omega^\pm(\sqrt{\nu})\, \mathrm{d}\nu\,. \tag{10}$$

† Since our scalar product is defined for real-valued functions, the projection of the Fourier transform $\boldsymbol{E}(\nu)$ implies thinking in terms of real-valued sine and cosine transforms. Integration restricted to $\nu \geqslant 0$ causes no loss of information since $\boldsymbol{E}(t)$ is real-valued.

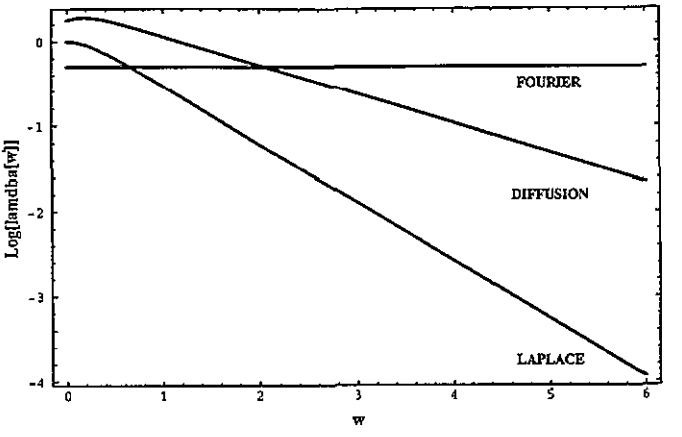

Figure 1. Eigenvalue spectra for different integral operators. The constant spectrum is for the Fourier transform while the most-decreasing one is for the Laplace transform. The spectrum labelled 'diffusion' corresponds to (9).

Provided that $\boldsymbol{E}(\nu)$ is noiseless and known for every $\nu \geqslant 0$, (10) gives the complete solution to our inverse problem. The eigenvalues $\lambda_\omega^\pm$ quantify the efficiency by which their corresponding eigenfunctions are transmitted into the data (see (6)): the larger the eigenvalue the more efficient the transmission of the information element. Eigenfunctions whose eigenvalues are too small become lost in the noise, and the process of dividing by such small eigenvalues in (10) will dramatically amplify any noise present in the data. Unfortunately, the spectrum (9) decays asymptotically to zero as $\omega \to \infty$ (figure 1), and this makes reconstruction (10) ill posed. Including the high-mode eigenfunctions in the solution will produce meaningless results, and our solution may be rewritten as the sum of two components,

$$\boldsymbol{U}(q) = \int_0^{\omega_{max}} \mathrm{d}\omega \frac{\Phi_\omega^\pm(q)}{\lambda_\omega^\pm} \int_0^\infty \boldsymbol{E}(\nu)\Phi_\omega^\pm\left(\sqrt{\nu}\right)\mathrm{d}\nu + \int_{\omega_{max}}^\infty \mathrm{d}\omega \frac{\Phi_\omega^\pm(q)}{\lambda_\omega^\pm} \int_0^\infty \boldsymbol{E}(\nu)\Phi_\omega^\pm\left(\sqrt{\nu}\right)\mathrm{d}\nu$$
$$= \boldsymbol{U}_\mathrm{d}(q) + \boldsymbol{U}_\mathrm{n}(q) \tag{11}$$

where the cutoff ω_{max} depends on the signal-to-noise ratio. The components $\boldsymbol{U}_\mathrm{d}(q)$ and $\boldsymbol{U}_\mathrm{n}(q)$ correspond respectively to the part of the solution which can be recovered from the data and to the one which cannot be. $\boldsymbol{U}_\mathrm{d}(q)$ is a low-pass filtered version of the true solution $\boldsymbol{U}(q)$ and is insufficient to allow for a high-resolution reconstruction. In fact, the resolution follows the distribution of the zero-crossings of $\Phi_{\omega_{max}}^\pm$ and rapidly deteriorates when q increases (figure 2). The only way to improve the resolution is to perform the inversion not only with data but also with some *a priori* information [34] whose role will be to extrapolate the reconstruction beyond the cutoff ω_{max}. From the point of view of inverse problem theory, this extrapolation may be considered as using *a priori* information to complete the basic solution $\boldsymbol{U}_\mathrm{d}(q)$ with a non-null $\boldsymbol{U}_\mathrm{n}(q)$ constructed in the null space generated by the basis $\{\Phi_\omega^\pm, \omega > \omega_{max}\}$.

3. Constraints and parametrization

The *a priori* information suitable to our inverse problem are of three types. The first constraint concerns the causality of the field $\boldsymbol{U}(q)$ and limits the support of the solution to $\mathbb{R}^+$.

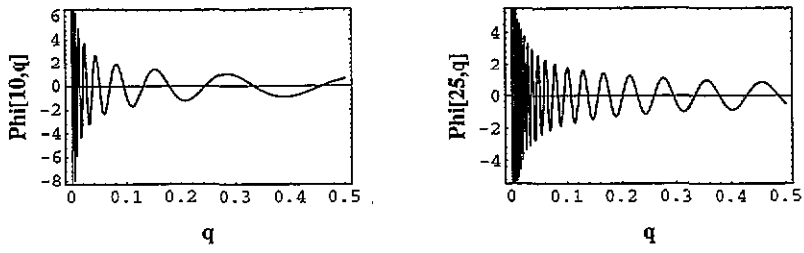

Figure 2. $\Phi_\omega^+(q)$ for $\omega = 10$ and $\omega = 25$.

A second constraint comes from the objectives of imaging which are of structural concern. In other words, the goal is to detect the edges of the more or less numerous homogeneous blocks which constitute the media to probe. This explains why the reflectivity is the right parameter to seek, since it is directly related to the edges of the structures where most of the jumps of the electromagnetic properties of the body occur. By definition these edges form a very sparse and irregular lattice in space which, thanks to the Huygens principle, will back-scatter sparse wavefronts when visited by an incident wavefront. As a consequence, and assuming an impulsive source term, $F(q)$, the sequences, $U(q)$, recorded at each receptor will be sparse trains of replicas of this initial short pulse (see numerical simulations in [37]). This will be true only for real reflection coefficients and, equivalently, if the incident wavefront attacks the edges of the structures under subcritical conditions. This allows the success of the seismic method under near-normal reflection conditions. Were these conditions to be violated, several reflection coefficients might become complex, and the corresponding reflected events would no longer be simple replicas of the source term [1]. In the remaining part of this discussion we shall assume that all reflection coefficients are real and that

$$U(q) = \sum_{n=1}^{N} U_n F(q - q_n) \tag{12}$$

is verified. Such a sparsity constraint upon the unknown field has been recognized to strongly stabilize ill-posed inverse problems similar to the present one [6]. Indeed, such a constraint has already successfully been applied to deconvolution of noisy seismic data [21]. The last constraint acts upon the nature of the source terms. If the electromagnetic source is known or if it is possible to deconvolve the data, which is merely the case in magnetotellurics, we may assume a Dirac impulse for the initial pulse $S(t)$. The corresponding propagative source term, $F(q)$, is also a Dirac impulse as is readily seen from (5) and (12) becomes

$$U(q) = \sum_{n=1}^{N} U_n \delta(q - q_n) \tag{13}$$

which, when inserted into (5), gives

$$E(\nu) = \sum_{n=1}^{N} U_n \exp\left(-q_n \sqrt{i\nu}\right). \tag{14}$$

In practice, the data are known for a finite set of discrete frequencies $\{E_{\text{data}}(\nu_1), E_{\text{data}}(\nu_2), \ldots, E_{\text{data}}(\nu_M)\}$ from which one has to get estimates of the unknown parameters $\{N, q_1, q_2, \ldots, q_N, U_1, U_2, \ldots, U_N\}$. This is the actual inverse problem which is discussed in the following section.

4. Computer implementation by simulated annealing

The inverse problem defined in the preceding section is linear with respect to the U_is and highly non-linear with respect to both the q_is and N as seen in (14). Provided a suitable frequency sampling, model (14) can be recast under the form of the Prony model [10] for which linearized sub-optimal solutions exist and whose lack of robustness is well known [14]. Indeed, we found that the presence of a very small noise in the data renders any linearized inversion impossible. This led us to attack the inverse problem with a fully non-linear strategy and, among the various powerful algorithms recently proposed, we retain simulated annealing [15] because of its clear theoretical links with the theory of inverse problems [34]. Although simulated annealing has the potential power to allow for a simultaneous inversion of all parameters, we preferred to decouple them, essentially because a simultaneous inversion implies the use of a multiparameter cost function whose components proved very difficult to balance. Since all parameters do not play the same role with respect to the inversion, we decoupled the algorithm into three main blocks. The first one consists of an analysis of the information content of the data set to estimate the number, N, of events to invert. Selecting this number is very important and makes the problem more stable. This is particularly true for Prony analysis [14] and, among the many ways to evaluate the order of Prony's model, we have found the spectral analysis of the data covariance matrix [35] a very efficient method [10]. Once we know how many reflectors are expected, we must locate them: this is our non-linear inverse problem. Simulated annealing uses an explicit computation of the cost function which allows for a decoupling between the U_is and the q_is. In practice we applied the simulated annealing algorithm to the restricted parameter set $\{q_1, q_2, \ldots, q_N\}$, and incorporated the linear parameters $\{U_1, U_2, \ldots, U_N\}$ into the cost function by computing them once a set of q_is had been selected. In the present study, the U_is are computed by numerically solving a Vandermonde system with standard least-squares techniques [18, 31]. This fixes the cost function to be the $\mathbb{L}_2$ norm defined by

$$S = \tfrac{1}{2} \sum_{m=1}^{M} \left[E_{\text{data}}(\nu_m) - E(\nu_m | q_1, q_2, \ldots, q_N) \right]^2 \tag{15}$$

and implies a Gaussian noise in the data for the inversion being optimal from a probabilistic point of view [34]. Just to make this section self-consistent, let us recall the basis of simulated annealing. The algorithm is a two-loop procedure whose inner loop consists of starting from a model $\{q_1, q_2, \ldots, q_N\}$ with cost S, then perturbing it to obtain $\{q'_1, q'_2, \ldots, q'_N\}$ with cost S', and finally retaining this new model with the probability $\mathcal{P} = \min[1, \exp(-(S' - S)/T)]$ where the parameter T, called the temperature for historical reasons, is kept fixed. Looping over this constitutes the Metropolis algorithm [24], and, provided there are a very large number of iterations, it can be shown that the sequence of accepted models satisfies the Boltzmann distribution, $\mathcal{P}_B = Z^{-1} \exp(-S/T)$, where Z is a normalizing partition function. The outer loop of simulated annealing is the cooling schedule which iterates over the Metropolis algorithm while the temperature is gradually lowered until no significant improvement occurs in the model perturbations. The two main questions to be answered when implementing the algorithm concern the lowering of the temperature in the cooling schedule and the way the parameter space is explored in the Metropolis algorithm. These two questions are addressed in the next two paragraphs.

The cooling schedule appears critical in the simulated annealing algorithm because it controls the overall convergence towards the best model. A too rapid decrease of the temperature will 'freeze' the solution into a local minimum of the cost function by forbiding

any tunelling effect which could allow the trapped model to escape from the local minimum. Conversely, a too slow decrease may result in prohibitive computational costs. Various cooling schedules have been proposed [16], and several studies [28, 25] about practical implementation of the simulated annealing algorithm favour the cooling schedule [12, 33]

$$T(n+1) = T(n) \exp\left(- \frac{\lambda T(n)}{\mathrm{sd}(S(n))} \right) \tag{16}$$

where λ is a parameter called the thermodynamic speed, and $\mathrm{sd}(S(n))$ is the standard deviation of the costs of the models accepted during the Metropolis algorithm at temperature $T(n)$. The choice of the value for λ is not crucial and we retain $\lambda = 0.75$. This cooling schedule is adaptive in the sense that the decrease of the temperature is slower when the models accepted during the preceding Metropolis loops have almost identical costs. In doing so, the schedule reiterates a sequence of Metropolis loops at an only-slightly lowered temperature such that the probability for an escape from an eventual local minimum is kept high. The initial temperature in this cooling schedule must be taken sufficiently high to allow for a wide exploration of the parameter space and the final temperature is set to one hundredth of the noise variance [10].

The second question to answer when implementing the algorithm is: how to perturb the current model to obtain the new model to be tested? Most applications of simulated annealing deal with (very large) discrete sets of models as, for instance, in combinatorial minimizations like the famous travelling salesman tour [15]. Such fundamentally discrete problems possess natural minimal increments and the difficulty is essentially how to combine them [8]. Many inverse problems, however, operate in continuous spaces where no 'atomic' minimum step may be simply defined. Choosing a too large *a priori* step-size in such a continuous space implies discretizing the parameter space with a coarse rigid frame which prevents any future fine zooming over the solution. Conversely, a too fine step-size produces an enormous number of models to visit and results in a dramatic decrease of the convergence rate analogous to the well known critical slowing-down phenomena encountered in Monte Carlo simulation [11]. This difficulty led several authors [36] to implement an adaptive-step version of simulated annealing by characterizing the local topology of the cost function from the size of the domain explored during the preceding Metropolis loops. In the same spirit, a merging of both the simulated annealing algorithm and the simplex method has recently been proposed [32]. The basic idea is to use simulated annealing to relax, more or less, the downhill updating in the simplex procedure which explores the continuous parameter space. This allows the simplex to escape from basins of attraction attached to local minima of the cost function by augmenting the costs of the vertices of the simplex while decreasing the costs of the attempted moves of the highest point of the simplex. From an intuitive point of view, we may conjecture that this procedure has the net effect of making the 'cost landscape' stochastically convex and, then, ensures convergence towards the absolute minimum. The main advantage of this algorithm is that it is free from any *a priori* discretization of the parameter space while it offers very attractive convergence rates.

5. A practical example

The algorithm described above has been tested with a 1D example previously inverted with a discretized version of simulated annealing [10]. The solutions are identical within the numerical accuracy interval. These tests show an important improvement of the convergence rates with the algorithm described in the present paper. The global behaviour

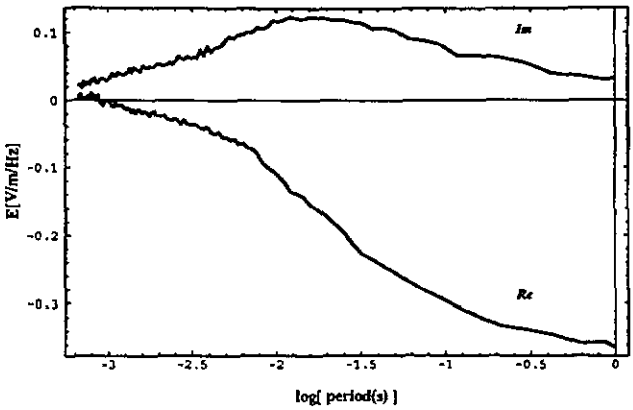

Figure 3. Pseudo-data for a station ($x = 750$ m) of the *en biseau* model (top of figure 4).

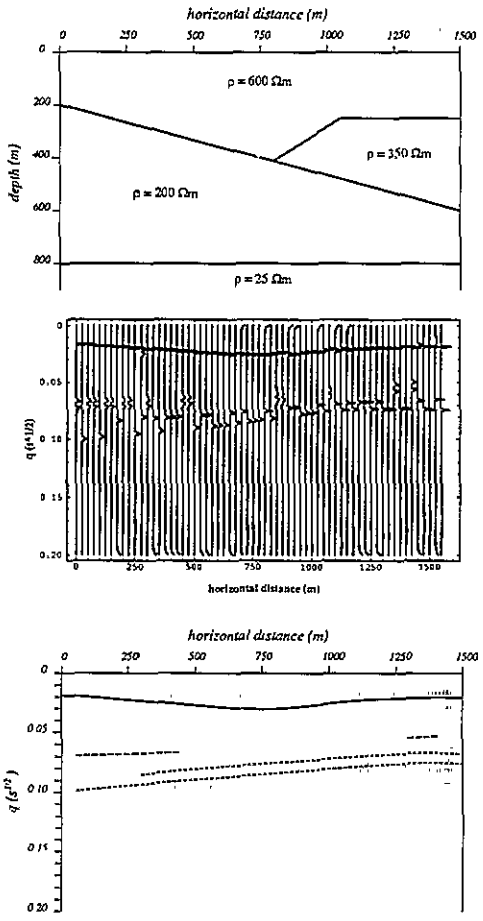

Figure 4. *En biseau* model. Top: sketch of the structure from which pseudo-data are computed. Middle, conditional probabilities of the inverted reflector. Bottom: main reflectors picked from the conditional-probability section.

of this algorithm follows what we described in our previous paper, namely a hierarchical determination of the parameters and a jump of the specific heat when approaching a parameter determination (see [10] for more details).

Two inversions of 2D models have been done. The first model consists of an *en biseau* structure (top of figure 4) from which we generated pseudo-magnetotelluric data at 63

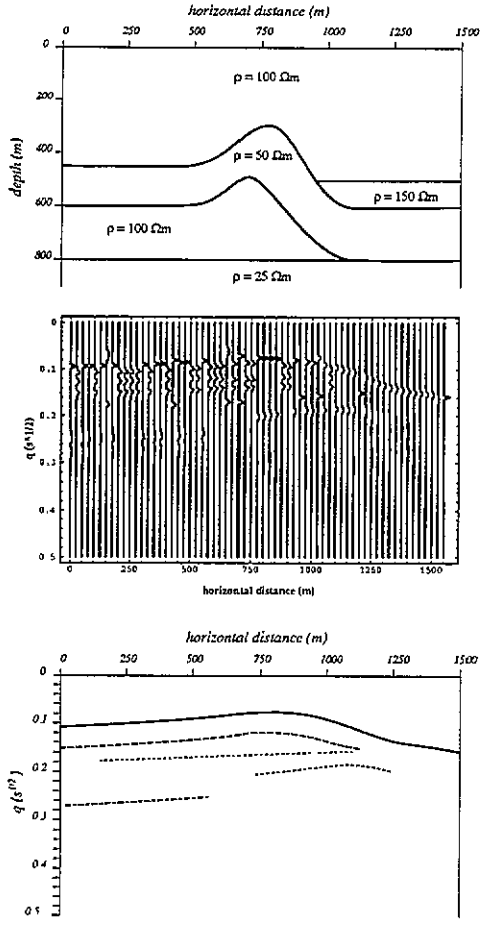

Figure 5. Anticlinal model. Top: sketch of the structure from which pseudo-data are computed. Middle: conditional probabilities of the inverted reflector. Bottom: main reflectors picked from the conditional-probability section.

equidistant stations along the surface. A finite-element program is used for this purpose [39]. The data for each station are computed for frequencies ranging from 1 to 1500 Hz with an additive white Gaussian noise ($\sigma^2 = 10^{-5}$) corresponding roughly to a signal-to-noise ratio of 30 dB (figure 3). Each trace is inverted independently and our inversion consists, in fact, of a succession of 1D inverse problems identical to the one recalled at the beginning of this section. The analysis of information content of the data indicates 3 events for almost all traces. Once the final temperature is reached, conditional probabilities

$$\mathcal{P}_A(q_n, k) = \frac{\exp(-S_k/T)}{\sum_{k=1}^{K} \exp(-S_k/T)} \tag{17}$$

are computed for $T = \sigma^2$. This allows evaluation of the uncertainties upon the location of the events (middle of figure 4).

This procedure furnishes an electromagnetic reflectivity (x, q) section analogous to the classical non-migrated seismic (x, t) images. Deriving an (x, z) section would involve a migration, a further step in the processing which has not yet been undertaken. Reflections from the first shallow interface are very well detected (bottom of figure 4) while deeper interfaces produce less strong, but coherent, wavefronts. A more complicated model consists of an anticlinal structure with a low-resistivity (i.e. low-velocity in the seismic sense) folded layer (top of figure 5). The conditional probabilities are more difficult to analyse (middle of

figure 5): the shallowest reflector remains well-detected but the deeper ones are somewhat interlaced and do not allow for a clear unambiguous interpretation (bottom of figure 5). This partial failure of the inversion appeals for a true 2D inverse algorithm which could ensure coherency between adjacent traces.

6. Conclusion

We have shown that reflectivity electromagnetic imaging in a diffusive context is possible provided a careful parametrization of the inverse problem is used. This demonstrates the importance of *a priori* information such as sparsity constraints which, however, make the inverse problem highly non-linear. Use of simulated annealing coupled with the simplex algorithm allows for a rapid convergence without neglecting resolution. Synthetic assessments of the method with pseudo-data show that good results are obtained whenthe data are corrupted with a reasonable amount of noise. More stable results could be reached if the inversions of section-traces could be performed simultaneously by accounting for some coherency criteria. This next step is in progress and will be described in a future paper.

Acknowledgments

The present study has been partly granted by the Centre National de la Recherche Scientifique (CNRS-INSU) via ATP 'Tomographie'. Discussions with Uriel Frisch, Dominique Lesselier, Douglas Oldenburg and Albert Tarantola strongly influenced and motivated our work. Most of the computations were done with the processing facilities of the 'Centre des Ressources Informatiques' from Université de Rennes 1. We are pleased to acknowledge Eric Picheral and François Dagorn for their technical support. A Mathematica [40] package implementing simulated annealing coupled with the simplex algorithm is available upon request to the authors.

References

[1] Aki K and Richards P G 1980 *Quantitative Seismology, Theory and Methods* (San Francisco: Freeman) vol I and II
[2] Bertero M, De Mol C, Gori F and Ronchi L 1983 Number of degrees of freedom in inverse diffraction *Opt. Acta* **30** 1051–65
[3] Bleistein N 1987 On the imaging of reflectors in the Earth *Geophys.* **52** 931–42
[4] Claerbout J 1990 *Imaging of the Earth's Interior* (Dordrecht: Reidel)
[5] Daniels D J, Gunton D J and Scott H E 1988 Introduction to subsurface radar *IEE Proc.* vol 135 pp 278–320
[6] Donoho D L 1992 Superresolution via sparsity constraints *SIAM J. Math. Anal.* **23** 1309–31
[7] Dziewonski A M and Woodhouse J H 1987 Global images of the Earth's interior *Science* **236** 37–48
[8] Ettelaie R and Moore M A 1987 Zero-temperature scaling and simulated annealing *J. Physique* **48** 1255–63
[9] Filippi P and Frisch U 1969 Relation entre l'équation de la chaleur et l'équationdes ondes de Helmholtz *C. R. Acad. Sci.* A **268** 804–7
[10] Gibert D and Virieux J 1991 Electromagnetic imaging and simulated annealing *J. Geophys. Res.* **96** 8057–67
[11] Gould H and Tobochnik J 1989 Overcoming critical slowing down *Comput. Phys.* **3** 82–6
[12] Huang M D, Romeo F and Sangiovanni-Vincentelli A L 1986 An efficient general cooling schedule for simulated annealing *Proc. IEEE Int. Conf. Computer-Aided Design (Santa Clara)* pp 381–4
[13] Jannane M *et al* 1989 Wavelengths of Earth structures that can be resolved from seismic reflection data *Geophys.* **54** 906–10
[14] Kay S M and Marple S L 1981 Spectrum analysis: a modern perspective *Proc. IEEE* **69** 1380–419
[15] Kirkpatrick S, Gelatt C D and Vecchi M P 1983 Optimization by simulated annealing *Science* **220** 671–80

[16] van Laarhoven P J and Aarts E H 1987 Simulated annealing: theory and applications *Mathematics and its applications* (Dordrecht: Reidel)
[17] Lavrent'ev M M, Romanov V G and Shishatskii S P 1980 *Ill-posed Problems of Mathematical Physics and Analysis* (Moscow: Nauka)
[18] Lawson C L and Hanson R L 1974 *Solving Least-squares Problems* (Englewood Cliffs, NJ: Prentice-Hall)
[19] Lee K H, Liu G and Morrison H F 1989 A new approach to modeling the electromagnetic response of conductive media *Geophys.* **54** 1180–92
[20] Lericolais G, Allenou J-P, Berné S and Morvan P 1990 A new system for acquisition and processing of very high-resolution seismic reflection data *Geophys.* **55** 1036–46
[21] Levy S and Fullagar P K 1981 Reconstruction of a sparse spike train from a portion of its spectrum, and application to high-resolution deconvolution *Geophys.* **46** 1235–43
[22] McWhirter J G and Pike E R 1978 On the numerical inversion of the Laplace transform andsimilar Fredholm integral equations of the first kind *J. Phys. A: Math. Gen.* **11** 1729–45
[23] McWhirter J G and Pike E R 1979 The extraction of information from laser anemometry data *Phys. Scr.* **19** 417–25
[24] Metrolopolis N, Rosenbluth A, Rosenbluth N, Teller A and Teller E 1953 Equation of state calculations by fast computing machines *J. Chem. Phys.* **21** 1087–92
[25] Mirkin G, Vasudevan K, Cook F A, Laidlawand W G and Wilson W G 1993 A comparison of several cooling schedules for simulated annealing implemented on a residual statics problem *Geophys. Res. Lett.* **20** 77–80
[26] Montagner J-P and Tanimoto T 1991 Global upper-mantle tomography of seismic velocities andanisotropies *J. Geophys. Res.* **96** 20337–51
[27] Morette-DeWitt C and Foong S K 1989 Path-integral solutions of wave equations with dissipation *Phys. Rev. Lett.* **62** 2201–4
[28] Mosegaard K and Vestergaard P D 1991 A simulated annealing approach to seismic model optimization with sparse prior information *Geophys. Prospecting* **39** 599–611
[29] Oristaglio M and Hohmann G W 1984 Diffusion of electromagnetic fields into a two-dimensional Earth: a finite-difference approach *Geophys.* **49** 870–94
[30] Ostrowsky N, Sornette D, Parker P and Pike E R 1981 Exponential sampling method for light scattering polydispersity analysis *Optica Acta* **28** 1059–70
[31] Press W H, Flannery B P, Teukolsky S A and Vetterling W T 1986 *Numerical Recipes* (Cambridge: Cambridge University Press)
[32] Press W H and Teukolsky S A 1991 Simulated annealing optimization over continuous spaces *Computers in Phys.* **5** 426–9
[33] Ruppeiner G 1988 Implementation of an adaptative, constant thermodynamic speed simulated annealing schedule *Nucl. Phys.* B *(Proc. Suppl.)* **5A** 116–21
[34] Tarantola A 1987 *Inverse Problem Theory* (Amsterdam: Elsevier)
[35] Van Blaricum M L and Mittra R 1978 Problems and solutions associated with Prony's method for processing transient data *IEEE Trans. Antennas Propag.* **26** 174–82
[36] Vanderbilt D and Louie S G 1984 A Monte Carlo simulated annealing approach to optimization over continuous variables *J. Comput. Phys.* **56** 259–71
[37] Virieux J 1986 P-SV wave propagation in heterogeneous media: velocity–stress finite-difference method *Geophys.* **51** 889–901
[38] Virieux J, Flores-Luna C and Gibert D 1994 Asymptotic theory for diffusive electromagnetic imaging *Geophys. J. Int.* in press
[39] Wannamaker P E, Stodt J A and Rijo L 1985 PW2D finite element program for solution of magnetotelluric responses of two-dimensional Earth resistivity structure *Technical Report* Earth Sci. Lab., University of Utah Research Institute
[40] Wolfram Research Inc. 1990 *Mathematica: a System for Doing Mathematics by Computer* Wolfram Research, Inc. Version 2.2
[41] Zorati R, Duchêne B, Lesselier D and Pons F 1991 Eddy current testing of anomalies in conductive materials: I. Qualitative imaging via diffraction tomography techniques *IEEE Trans. Magn.* **27** 4416–37
[42] Zorati R, Duchêne B, Lesselier D and Pons F 1992 Eddy current testing of anomalies in conductive materials: II. Quantitative imaging via deterministic and stochastic inversion techniques *IEEE Trans. Magn.* **28** 1850–62